Reprint

Water-Assisted Concerted Proton-Electron Transfer at Co(II)-Aquo Sites in Polyoxotungstates With Photogenerated Ru^III(bpy)_3^{3+} Oxidant

Francesco Rigodanza,[a, b] Nadia Marino,*[c] Alessandro Bonetto,[d] Antonio Marcomini,[d] Marcella Bonchio,*[a, b] Mirco Natali,*[e] and Andrea Sartorel*[a]

The cobalt substituted polyoxotungstate $[Co_6(H_2O)_2(\alpha\text{-}B\text{-}PW_9O_{34})_2(PW_6O_{26})]^{17-}$ (**Co6**) displays fast electron transfer (ET) kinetics to photogenerated Ru^III(bpy)_3^{3+}, 4 to 5 orders of magnitude faster than the corresponding ET observed for cobalt oxide nanoparticles. Mechanistic evidence has been acquired indicating that: (i) the one-electron oxidation of **Co6** involves Co(II) aquo or Co(II) hydroxo groups (abbreviated as **Co6(II)**–OH_2 and **Co6(II)**–OH, respectively, whose speciation in aqueous solution is associated to a pK_a of 7.6), and generates a Co(III)–OH moiety (**Co6(III)**–OH), as proven by transient absorption spectroscopy; (ii) at pH > pK_a, the **Co6(II)**–OH→Ru^III(bpy)_3^{3+} ET occurs via bimolecular kinetics, with a rate constant k close to the diffusion limit and dependent on the ionic strength of the medium, consistent with reaction between charged species; (iii) at pH < pK_a, the process involves **Co6(II)**–OH_2→**Co6(III)**–OH transformation and proceeds via a multiple-site, concerted proton electron transfer (CPET) where water assists the transfer of the proton, as proven by the absence of effect of buffer base concentrations on the rate of the ET and by a H/D kinetic isotope in a range of 1.2–1.4. The reactivity of water is ascribed to its organization on the surface of the polyanionic scaffold through hydrogen bond networking involving the Co(II)–OH_2 group.

[a] Dr. F. Rigodanza, Prof. M. Bonchio, Prof. A. Sartorel
Department of Chemical Sciences,
University of Padova
via Marzolo 1, 35131 Padova, Italy
E-mail: marcella.bonchio@unipd.it
andrea.sartorel@unipd.it

[b] Dr. F. Rigodanza, Prof. M. Bonchio
Consiglio Nazionale delle Ricerche (C.N.R.),
Institute on Membrane Technology section of Padova
via Marzolo 1, 35131 Padova, Italy

[c] Prof. N. Marino
Department of Chemistry and Chemical Technologies,
University of Calabria
87036 Arcavacata di Rende (CS), Italy
E-mail: nadia.marino@unical.it

[d] Dr. A. Bonetto, Prof. A. Marcomini
Dept. Environmental Sciences, Informatics and Statistics,
University Ca' Foscari Venice Vegapark
Via delle Industrie 21/8, 30175 Marghera, Venice, Italy

[e] Prof. M. Natali
Department of Chemical, Pharmaceutical and Agricultural Sciences (DOCPAS),
University of Ferrara, and Centro Interuniversitario per la Conversione Chimica dell'Energia Solare (SOLARCHEM) sez. di Ferrara
via L. Borsari 46, 44121 Ferrara, Italy
E-mail: mirco.natali@unife.it

1. Introduction

Proton coupled electron transfer (PCET) is one fundamental process regulating biological functions such as respiration and photosynthesis.[1–6] Synthetic systems have been extensively investigated where PCET is central for energy conversion schemes and small molecule activation.[7–9] When PCET is driven at metal cores, it is often associated to proton dissociation of an acidic ligand.[10–12]

In particular, electron and proton transfers involving cobalt sites as donors often involve a Co(II)→Co(III) or a Co(III)→Co(IV) state transition, triggering the conversion of apical waters from aquo→hydroxo and/or hydroxo→oxo ligands.[13,14]

Of specific relevance is the reactivity of cobalt sites towards photogenerated one-electron oxidants, as in the case of Ru^III(bpy)_3^{3+} (bpy=2,2'-bipyridine). Ru^III(bpy)_3^{3+} can be photogenerated with high quantum yield ($\phi \s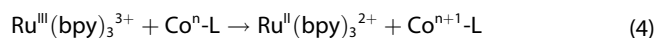im 2$) by irradiating the Ru^II(bpy)_3^{2+} precursor ($\varepsilon^{450}=1.4\times10^4$ M^{-1}cm^{-1}, lifetime of the triplet excited state up to hundreds of ns in aqueous solutions[15]) in the presence of $S_2O_8^{2-}$ as the primary acceptor according to equations 1–3.[16–18] Ru^III(bpy)_3^{3+} can then operate as one electron acceptor ($E=1.26$ vs NHE for the Ru(III/II) couple) from the Co^n-L site, generating a Co^{n+1}-L species (eq. 4, where n and n+1 are the oxidation states of the cobalt center and L generally indicates an aquo, hydroxo or oxo ligand).

$$Ru^{II}(bpy)_3^{2+} + h\nu \rightarrow {}^*Ru^{II}(bpy)_3^{2+} \tag{1}$$

$$^*Ru^{II}(bpy)_3^{2+} + S_2O_8^{2-} \rightarrow Ru^{III}(bpy)_3^{3+} + SO_4^{-} + SO_4^{2-} \tag{2}$$

$$Ru^{II}(bpy)_3^{2+} + SO_4^{-} \rightarrow Ru^{III}(bpy)_3^{3+} + SO_4^{2-} \tag{3}$$

ChemPhysChem

Articles
doi.org/10.1002/cphc.202100190

Chemistry
Europe
European Chemical
Societies Publishing

$$Ru^{III}(bpy)_3^{3+} + Co^n\text{-}L \rightarrow Ru^{II}(bpy)_3^{2+} + Co^{n+1}\text{-}L \qquad (4)$$
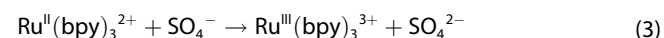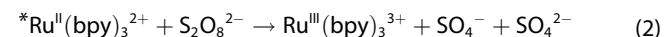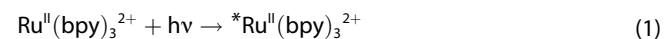
Previous studies by our group showed a fast, diffusion-controlled process for eq. 4 when the Co-aquo site is embedded in polyoxometalate (POMs) $(k > 10^9 \text{ M}^{-1}\text{s}^{-1})$.[19,20] This rate is strongly enhanced with respect to cobalt coordination complexes with organic ligands $(k \approx 10^8 \text{ M}^{-1}\text{s}^{-1})$,[21] and overarches by several orders of magnitude that of cobalt oxide nanoparticles (k in the range 10^4 to $10^5 \text{ M}^{-1}\text{s}^{-1}$).[20,22]

POMs have been often considered as molecular models of metal oxides surfaces, and indeed the oxygen-based coordination environment of cobalt in POMs is reminiscent of the one observed in cobalt oxides.[23–27] Therefore, the origin of such a peculiar reactivity of cobalt POMs with $Ru^{III}(bpy)_3^{3+}$ is worth of deeper investigation, since a detailed mechanistic comprehension of the nature of this ET process is still elusive.

We report herein the ET dynamics driven by photogenerated $Ru^{III}(bpy)_3^{3+}$ and involving the Co-substituted polyoxotungstate $[Co_6(H_2O)_2(\alpha\text{-B-PW}_9O_{34})_2(PW_6O_{26})]^{17-}$ (**Co6**).[28–30]

Our results allow to evaluate the impact of several effectors on PCET phenomena, including the solution pH, buffer type and concentration, and ionic strength of the medium.[22,29,30] **Co6** has been identified as a suitable platform for PCET studies considering that: (i) the POM structure displays two equivalent Co^{II}-aquo moieties as competent sites for a systematic evaluation of ET, possibly related to the transfer of protons; (ii) differently from other POM analogs,[31–33] **Co6** is sufficiently stable in aqueous solution towards Co(II) ions leaching (*vide infra*) thus providing a benchmark Co-POM system under different experimental conditions; (iii) H-bonded domains are located in ideal proximity to the Co-aquo sites, that happen to be involved in the formation of water channels at the POM surface. Converging evidence is acquired that points to a fast PCET regime assisted by water, that turns out to be the competent proton acceptor, favored by stabilization of H-bonding networks at the POM surface. The unique role of water channels has been highlighted in the seminal studies of Jean Michel Savéant, addressing the bio-inspired relevance of PCET mechanisms.[1]

2. Results and Discussion

2.1. Synthesis and Characterization at the Solid State of Co6[28–30] (XRD, ICP-MS, IR)

Deep purple, sharp rod-shaped crystals of $[Co_6(H_2O)_2(\alpha\text{-B-PW}_9O_{34})_2(PW_6O_{26})]^{17-}$ (**Co6**) as the sodium salt were obtained by refluxing in aqueous solution (pH in the range 5.5–7.0) a Co(II) precursor in the presence of tungstate and phosphate ions (see the supporting information for more details on the synthesis).[29]

The identity of the crystals of **Co6** was unambiguously established through both single-crystal (XRD) and powder (PXRD) X-ray diffraction. Representative cell parameters obtained by XRD analysis, consistent with those reported for **Co6** are:[29] $a = 17.692(3)$, $b = 22.289(2)$, $c = 34.926(4)$ Å; $\beta =$ 96.005(17)°; $V = 13697(3)$ Å^3; monoclinic space group $P2_1/c$. PXRD patterns are reported in the supporting information.

Co6 has a peculiar, "banana-shaped" structure[29] with two identical and specular $\{Co_3O_{13}\}$ cores sandwiched between two $[\alpha\text{-B-PW}_9O_{34}]^{9-}$ units (one each) and a $[B\text{-PW}_6O_{26}]^{11-}$ polyoxoanion fragment (Figure 1a). Of relevance to this work is to focus on the two *cis* Co(II)-aquo groups featured by the molecular anion, since such type of moieties have been previously shown to be relevant in photoinduced ET processes to $Ru^{III}(bpy)_3^{3+}$.[19] We note that two weak intramolecular hydrogen-bonds are likely to be established by each of the two terminally Co-coordinated water molecules towards just ideally located W=O moieties of the central $[B\text{-PW}_6O_{26}]^{11-}$ unit of **Co6** (see Figure 1a; O–O distances of 3.11–3.12 Å are indicated by dashed lines). More interestingly, several crystallization water molecules surround the polyoxoanion in the solid state, some of them being close enough to the Co(II)-aquo groups to be able to establish intermolecular H-bonds competing with the intramolecular ones previously mentioned (Figure 1b). A projection along the crystallographic [1 0 ½] direction of a portion of the crystal packing of **Co6**,[29] depicted in Figure S2, clearly shows a 2D hexagonal packing of the polyoxoanions wrapped up by the crystallization water molecules and the sodium countercations. A certain degree of organization of water molecules on the POM surface is expected to be maintained also in solution, in particular through solvation of terminal W=O sites involving H-bonds;[34,35] their role in the reactivity pertinent to this work is fundamental, and will be further discussed along the manuscript (*vide infra*).

In the solid state structure of **Co6**,[29] the crystallization water molecules appear not just extensively H-bonded to the molecular anions, but also plausibly involved in the formation of several "water channels" (see Figure S2). A close-look to the Co(II)–OH$_2$ moieties immediate surroundings, reveals indeed the existence of water channels possibly including the coordinated water molecules (see Figure 1b).

The identity of **Co6** was further confirmed by inductively coupled plasma mass spectrometry (ICP-MS), FT-IR and UV-Vis analyses. ICP analysis of **Co6** crystals, reveal a Co amount of $4.81 \pm 0.13\%$ w/w (calc. 4.84) and a W amount of $56.2 \pm 1\%$ w/w (calc. 60.4; the recovery of tungsten was not complete, showing a $<10\%$ loss with respect to calculated values, as verified also with other Co-POMs, see table S1 in Supporting Information). The FT-IR spectrum of a **Co6** sample shows bands at 1030, 933, 899–802 and 733 cm^{-1}, assigned to the P–O, W=O$_t$ (O$_t$ = terminal oxygen), W–O$_b$ (O$_b$ = bridging oxygen in corner sharing octahedra), and W–O$_c$ (O$_c$ = bridging oxygen in edge sharing octahedra) stretching modes, respectively (Figure S5).[29,30]

In aqueous phosphate buffer, **Co6** shows an absorption band centered at 562 nm ($\varepsilon^{562} = 280 \text{ M}^{-1}\text{cm}^{-1}$), attributed to Co based d-d transitions, Figure 2. In addition, the intensity of the UV-Vis trace undergoes only a slight abatement ($<1\%$ after 1 h), confirming a good stability of **Co6** in this medium.[31,33,36] The slight decrease of the absorption is ascribed to the release of Co(II) ions in the aqueous solution,[31,33,36] as proven by ^{31}P NMR line broadening experiments: the full-width at half

ChemPhysChem

Articles
doi.org/10.1002/cphc.202100190
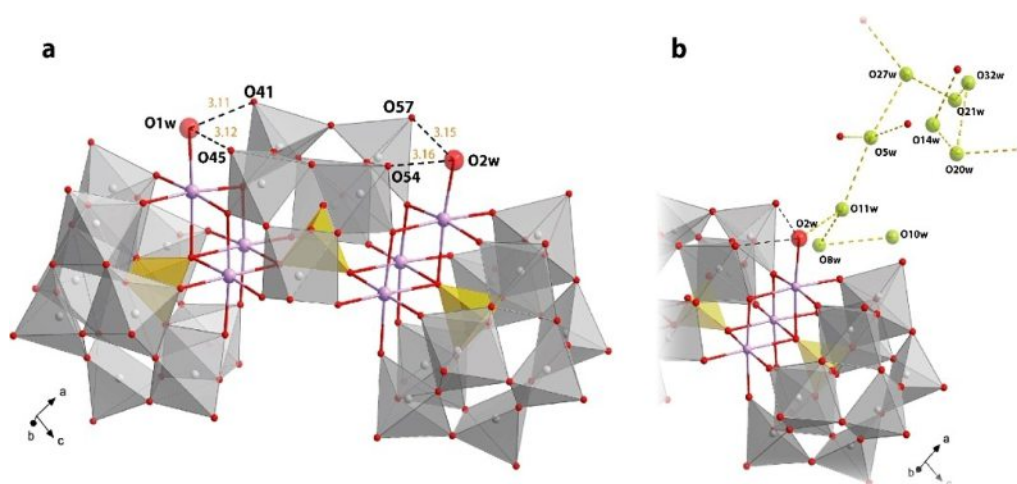
Chemistry
Europe
European Chemical
Societies Publishing

Figure 1. Left: molecular structure of the anionic "banana-shaped" **Co6** POM as found in the solid-state structure of $Na_7H_{10}[Co_6(H_2O)_2(\alpha-B-PW_9O_{34})_2(PW_6O_{26})] \cdot 31$ H_2O (**Na$_7$H$_{10}$Co6**, CSD 423955, Ref. [29]). Color and model codes: W atoms = grey spheres and polyhedra; P atoms = yellow polyhedra; Co = violet spheres; O_{POM} atoms = small red spheres; terminally Co-coordinated water molecules = large red spheres. Plausible, weak intramolecular H-bonds between the terminally coordinated water molecules and vicinal POM-embedded W=O moieties are depicted as black dashed lines (the indicated $O_w \cdots O=W$ distances are in Å). Right: detailed view of one of the two Co(II)–OH$_2$ moieties of **Co6** in its immediate environment, highlighting the H-bonding network established with and between the nearest crystallization water molecules (approximate $O_w \cdots O_w$ distances in Å: O2w⋯O11w 3.16, O11w⋯O8w 3.19, O8w⋯O10w 3.18, O11w⋯O5w 3.17, O5w⋯O27w 2.98, O27w⋯O21w 3.05, O21w⋯O32w 3.02, O32w⋯O20w 3.18, O20w⋯O14w 3.04). Sodium cations, crystallization water molecules not directly H-bonded to the selected network as well as vicinal **Co6** POMs are not shown for clarity. The number of Na counterions of **Co6** can vary depending on the crystallization conditions, with protons accounting for the complementary charge balance: in the present work, the ICP-MS analysis indicate a counter-ion composition compatible with a Na$_{15}$H$_2$**Co6** formulation, see table S1 in supporting information; the protons acting as counter cations are likely bound to oxygen of the POM scaffold,[35b] and can participate in the H-bonding of water molecules.

|	
Table 1. Rate and equilibrium constants discussed in the present work.	
k_{obs}	Unimolecular, pseudo first order rate constant for the reactivity of **Co6** with Ru^{III}(bpy)$_3^{3+}$; determined from mono exponential fitting of the flash photolysis traces. First order in [Ru^{III}(bpy)$_3^{3+}$].
k	Bimolecular rate constant for the reactivity of **Co6** with Ru^{III}(bpy)$_3^{3+}$; first order in [Ru^{III}(bpy)$_3^{3+}$] and [**Co6**].
k_1	Bimolecular diffusion constant for the formation of the encounter complex (eq. 5); first order in [Ru^{III}(bpy)$_3^{3+}$] and [**Co6**].
k_{-1}	Unimolecular rate constant for the backward dissociation of the encounter complex into the reactants (eq. 5).
k_2	Unimolecular rate constant for the formation of the successor complex from the encounter complex (eq. 6). It involves an ET and a CPET in the cases of **Co6**–**OH** and **Co6**–**OH$_2$**, respectively.
k_{-2}	Unimolecular rate constant for the backward conversion of the successor complex into the encounter complex (eq. 6). It is pH dependent in the case of a CPET, since H$_3$O$^+$ is a reactant.
k_3	Unimolecular rate constant for the product diffusion from the successor complex (eq. 8).
K_a	Acid dissociation constant of **Co6(II)**–**OH$_2$**, $K_a = 10^{-7.6}$.
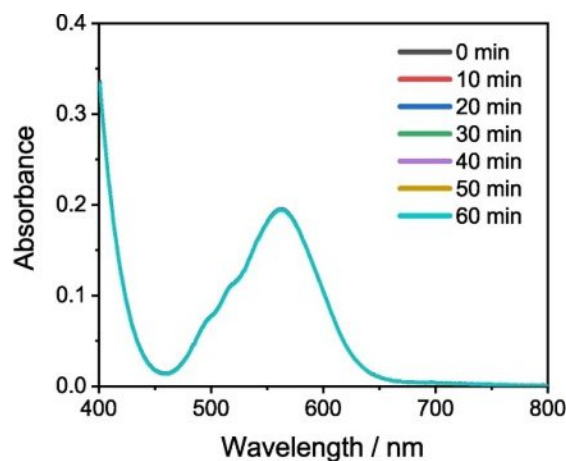
Figure 2. UV-Vis spectra of **Co6** over time: 0.70 mM **Co6** (5 mg/ml), in 30 mM phosphate buffer, pH 8, 25 °C.

maximum (FWHM) of the phosphate ^{31}P NMR signal is indeed linearly dependent on *free* Co(II) aqueous ions (see NMR spectra and calibration curve in Figure S7 in supporting information),[37] and confirms a minor release of ca 1.25% of the total Cobalt content from **Co6** after 2 h, and of 2.1% over 6 hours in phosphate buffer at pH 8 (Figure S7 in supporting information).

The redox properties of **Co6** were investigated by means of cyclic voltammetry, in 0.1 M aqueous phosphate electrolyte, in the pH range 3.7–8.9, and focusing on the anodic scan. The CV traces show a quasi-reversible redox process (Figure 3, top), attributed to oxidation of Co(II) to Co(III), where the apparent $E_{1/2}$ shows a pH dependence (Figure 3): in particular, in the pH range 3.7–7.6 the $E_{1/2}$ decreases linearly with pH with a slope of

65 ± 5 mV per pH unit. This observation is consistent with a PCET oxidation of Co^{II}–OH$_2$ into Co^{III}–OH, involving the **Co6** POM sites.[38] At pH > 7.6 the Co(III/II) $E_{1/2}$ is not pH dependent anymore, which is ascribable to one-electron oxidation of Co^{II}–OH into Co^{III}–OH.[39,40]

The dependence of the Co(III/II) potential on pH registered for **Co6**, is consistent with the Pourbaix diagram reported for other Co species,[40,41] and is summarized in Scheme 1, where the Co^{II}–OH$_2$/Co^{II}–OH equilibrium in **Co6** is associated to a pKa ~ 7.6 (structurally related Co^{II}-aqua moieties embedded in polyoxometalates show pK$_a$ of ca 8,[42] while Co^{II}–OH$_2$ group

ChemPhysChem

Articles
doi.org/10.1002/cphc.202100190

**Chemistry
Europe**
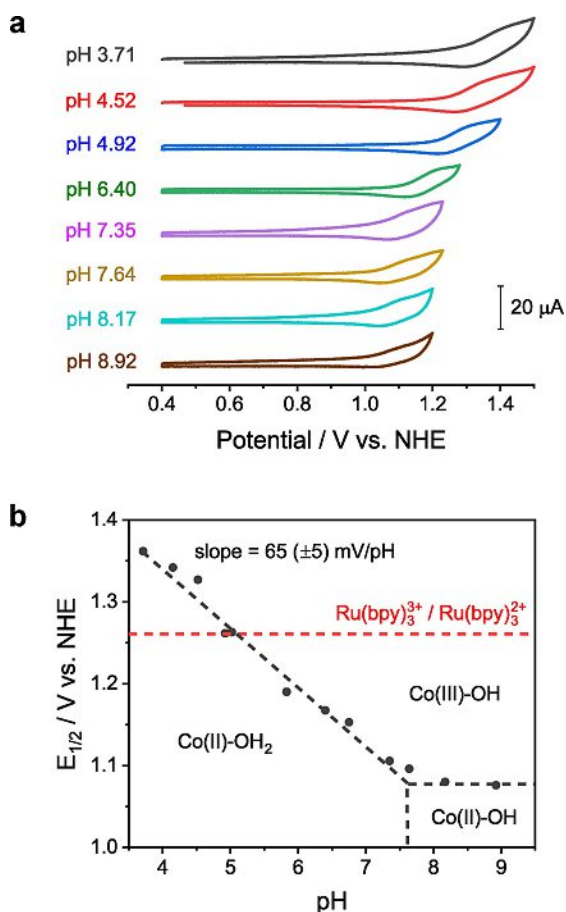European Chemical
Societies Publishing

Figure 3. a) Cyclic voltammetries under anodic scan of 1 mM **Co6** in 0.1 M phosphate electrolyte, pH 3.71–8.92 (representative traces). Glassy carbon (GC) working electrode, Pt counter electrode, Ag/AgCl reference electrode. Potentials are converted versus NHE with the following equation E vs NHE = E vs Ag/AgCl + 0.197 V. The analysis is limited in the pH window 3.71–8.92; below pH 3.7 the solution of **Co6** visibly changes color switching from purple to light pink, suggesting decomposition of **Co6**. b) Pourbaix diagram for the Co(II)/Co(III) species.
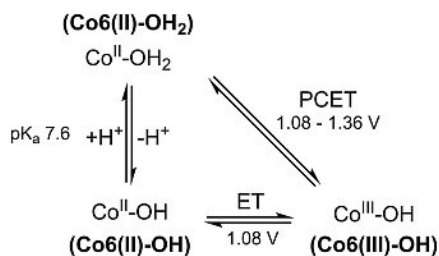
Scheme 1. Representation of acid base and Co(III/II) redox processes in **Co6**, involving oxidation of $Co^{II}-OH_2$ or $Co^{II}-OH$ moieties to $Co^{III}-OH$. PCET: proton coupled electron transfer; ET: electron transfer. Potentials are reported versus normal hydrogen electrode, NHE.

embedded in a N_2O_2 Schiff based salophen ligand displays a $pK_a = 6.4^{[21]}$). In the explored pH range, the Co^{III} oxidized form bears a hydroxyl apical ligand, as expected from the higher acidity of Co^{III} aquo moieties with respect to Co^{II} (for Ru and Mn aquo complexes, the difference in pK_a between the III/II state is about 9–10 units).[2,43]
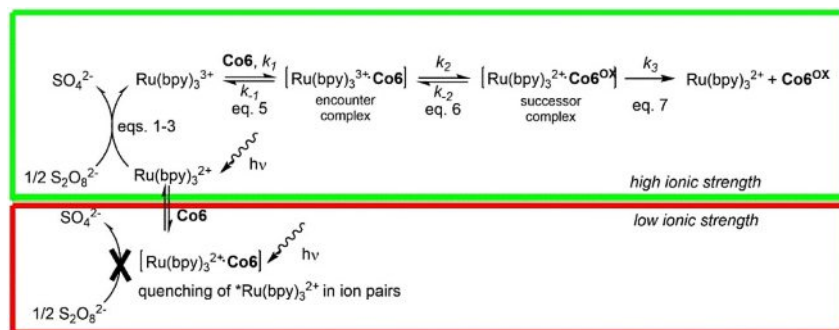
For the sake of simplicity, the POM embedded cobalt sites will be abbreviated as **Co6(II)—OH₂**, **Co6(II)—OH** and **Co6(III)—OH** (see Scheme 1).

Under all the conditions explored, the first Co(III/II) wave is thus observed in the range 1.08–1.36 V vs NHE, followed by a second, intense and irreversible wave, whose onset potential also shows pH dependence (Figure S8 in Supporting Information). As confirmed by controlled potential electrolysis (Figure S9 in Supporting Information) this process is associated to electrodeposition of cobalt oxide based materials from **Co6** precursor, being responsible for the electrocatalytic oxygen evolution at > 1.3 V vs NHE at pH 8 (observed with a faradaic yield of 70%); consistently, the UV-Vis traces of the **Co6** in solution show a marked change along the electrolysis (Figure S9 in Supporting Information).[20]

2.2. Ion Pairing with $Ru(bpy)_3^{2+}$

When polyanionic, POMs are used in combination with $Ru(bpy)_3^{2+}$ or other cationic sensitizers, the formation of ion pairs, is responsible for the precipitation of amorphous aggregates.[19,20,44–47] The formation of $Ru(bpy)_3^{2+}$/**Co6** ionic aggregates occurs with an average 6:1 stoichiometry as indicated by conductometric titration experiments of **Co6** in water upon addition of $Ru(bpy)_3^{2+}$ aliquots (added as the dichloride salt, Figure S10 in Supporting Information).

The ionic association is further confirmed by the absorption spectrum of a $Ru(bpy)_3^{2+}$/**Co6** adducts in water, showing a slight decrease (< 5%) of the intensity of the $Ru(bpy)_3^{2+}$ metal-to-ligand charge transfer (MLCT) band at 450 nm, and the growth of a broad absorption at longer wavelengths (Figure S11 in Supporting Information). In the presence of **Co6**, a major abatement of the $Ru(bpy)_3^{2+}$ luminescence is also observed (Figure S12 in Supporting Information), accompanied by a ca 15 nm red shift of the emission maximum. These spectral changes are compatible with those observed for ion-paired adducts between $Ru(bpy)_3^{2+}$ and polyoxomolybdate anions and are ascribed to a favored intramolecular quenching pathway by the co-localized **Co6** polyanion within the aggregate (Scheme 2).[48,49] Concerning the quenching mechanism, an oxidative pathway (i.e., oxidation of $*Ru^{II}(bpy)_3^{2+}$ to $Ru^{III}(bpy)_3^{3+}$ accompanied by reduction of **Co6**) followed by back electron transfer can be likely envisaged from previous studies on $Ru(bpy)_3^{2+}$/POM adducts,[19,45,48,49] although energy transfer from $*Ru^{II}(bpy)_3^{2+}$ to cobalt low-lying d-d states cannot be ruled out. The electrostatic nature of the $Ru(bpy)_3^{2+}$/**Co6** adducts is also corroborated by the recovery of the luminescence behavior upon addition of Na_2SO_4. As a matter of fact, $Ru(bpy)_3^{2+}$ emission recovers and blue-shifts upon increasing the ionic strength of the aqueous medium, which is consistent with ion pair dissociation (Figure S12 in Supporting Information).[19,20,44–47] Quenching of $*Ru(bpy)_3^{2+}$ excited state by **Co6** within ion-paired adducts (red frame in Scheme 2) is expected to counteract the photochemical reaction with persulfate and the
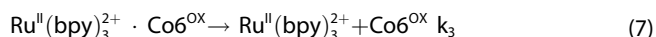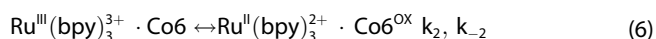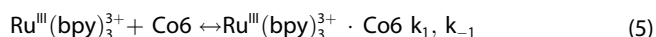
ChemPhysChem

Articles
doi.org/10.1002/cphc.202100190

Chemistry
Europe
European Chemical
Societies Publishing

Scheme 2. Schematic representation of photochemical events within the **Co6**/Ru(bpy)$_3^{2+}$/S$_2$O$_8^{2-}$ system: quenching of *Ru(bpy)$_3^{2+}$ within **Co6** Ru(bpy)$_3^{2+}$ ion pairs (red frame); photogeneration of Ru(bpy)$_3^{3+}$ via reaction with persulfate, and subsequent **Co6**→ Ru(bpy)$_3^{3+}$ ET reactivity (green frame).

consequent production of Ru(bpy)$_3^{3+}$ (equations 1–3). In this respect, photogeneration of Ru(bpy)$_3^{3+}$ has been conducted under high ionic strength conditions, in the presence of an electrolyte buffer (1–100 mM) and 5 mM sodium persulfate (green frame in Scheme 2).

2.3. Reactivity of Co6 With Photogenerated Ru^{III}(bpy)$_3^{3+}$

Under bimolecular conditions, the **Co6**→Ru^{III}(bpy)$_3^{3+}$ ET can be rationalized using a classical kinetic model that foresees the formation of an encounter complex, eq 5, followed by ET to form the successor complex, eq 6, and product diffusion, eq 7, green frame in Scheme 2 (**Co6**^{OX} indicates the oxidized form of **Co6**).[50] Accordingly, assuming the steady-state approximation for the encounter and successor complexes, Ru^{III}(bpy)$_3^{3+}$·**Co6** and Ru^{II}(bpy)$_3^{2+}$·**Co6**^{OX}, the k of the whole reaction can be described by equations 8 and 9 (see details of the treatment in supporting information).[50]

$$Ru^{III}(bpy)_3^{3+} + Co6 \leftrightarrow Ru^{III}(bpy)_3^{3+} \cdot Co6 \quad k_1, k_{-1} \tag{5}$$

$$Ru^{III}(bpy)_3^{3+} \cdot Co6 \leftrightarrow Ru^{II}(bpy)_3^{2+} \cdot Co6^{OX} \quad k_2, k_{-2} \tag{6}$$

$$Ru^{II}(bpy)_3^{2+} \cdot Co6^{OX} \rightarrow Ru^{II}(bpy)_3^{2+} + Co6^{OX} \quad k_3 \tag{7}$$

$$ET \ rate = k \times [Ru(bpy)_3^{3+}] \times [Co6] \tag{8}$$

$$k = \frac{k_1}{[1 + (1 + k_{-2}/k_3) \times k_{-1}/k_2]} \tag{9}$$

$$k \approx k_1 \quad if \ k_3 \gg k_{-2} \ and \ k_2 \gg k_{-1} \tag{10}$$

$$ET \ rate = -\frac{d[Ru(bpy)_3^{3+}]}{dt} = k_{obs} \times [Ru(bpy)_3^{3+}] \tag{11}$$

When the forward step in equation 6 is much faster than the reverse step in eq 5 ($k_2 > k_{-1}$), and the step in eq 7 is much faster than the reverse step in eq 6 ($k_3 > k_{-2}$), eq 9 simplifies into eq 10, with k_1 being characteristic of a diffusion-controlled process.

The photogeneration of Ru^{III}(bpy)$_3^{3+}$ in the presence of persulfate (according to equations 1–3) and its reaction with **Co6** (equations 5–7) have been conveniently followed by laser flash photolysis upon excitation at 355 nm. Formation of Ru^{III}(bpy)$_3^{3+}$ via oxidative quenching by persulfate in 50 mM phosphate buffer (pH 8) is detected from its transient absorption spectrum displaying the bleaching of the metal-to-ligand charge transfer (MLCT) transition at 450 nm (Figure 4a, black trace). Reaction of Ru^{III}(bpy)$_3^{3+}$ with **Co6** in the μs time scale is then accompanied by the recovery of the MLCT absorbance at 450 nm, due to the repopulation of the ground state Ru^{II}-(bpy)$_3^{2+}$, and by the concurrent formation of a residual positive absorption with a maximum centered at 520 nm (Figure 4a, red and blue traces) ascribable to the **Co6(III)**–**OH** as predicted by the cyclic voltammetry analysis discussed above (Figure 3). It is worth noting that **Co6(III)**–**OH** can be obtained also by the reaction of **Co6** with the sulfate radical,[45] in particular under operating conditions where the concentrations of **Co6** and of Ru(bpy)$_3^{2+}$ are similar. This possible reactivity however does not significantly impact on the determination of the rate constants as it is further discussed in the manuscript (*vide infra*).

The kinetics of the ET reaction from **Co6** to the photogenerated Ru^{III}(bpy)$_3^{3+}$ have been then monitored in a time-scale of 50 μs following the evolution of the transient absorption signal at 450 nm over time (Figure 4b). By working at different concentrations of **Co6** and operating under pseudo first order kinetic conditions (i.e., photogenerated [Ru^{III}(bpy)$_3^{3+}$] ≪ [**Co6**]) it is possible to fit the MLCT recovery with mono exponential functions (Figure 4b), thus providing the observed pseudo first order rate constant k_{obs} of the process (eq. 11). Importantly, the first order dependence of the k_{obs} vs. **Co6** concentration (Figure 5a) clearly confirms the bimolecular nature of the ET event between Ru^{III}(bpy)$_3^{3+}$ and **Co6**, thus ruling out any effect on the ET rate due to static quenching phenomena within ion-paired sensitizer/catalyst adducts (see above). Thus, bimolecular k can be obtained by the slope of the linear fitting of k_{obs} vs the concentration of **Co6** (Figure 5a). Under the experimental conditions described in Figure 4 (50 mM phosphate buffer at pH 8), where [**Co6(II)**–**OH**] ≫ [**Co6(II)**–**OH**$_2$], a bimolecular rate constant $k = 2.8 \ (\pm 0.1) \cdot 10^9 \ M^{-1} s^{-1}$ is obtained, consistent with a diffusion-controlled ET process
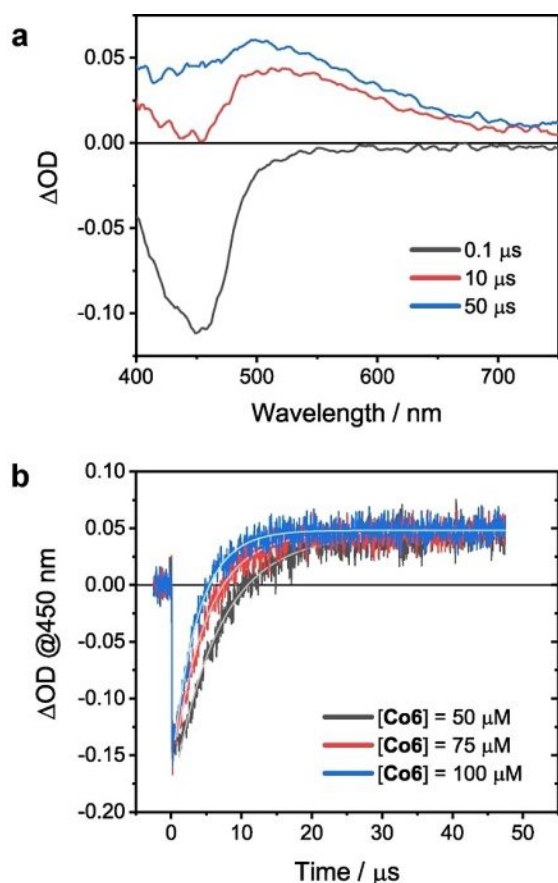
ChemPhysChem

Articles
doi.org/10.1002/cphc.202100190

Chemistry
Europe
European Chemical
Societies Publishing

Figure 4. a) Transient absorption spectra obtained by laser flash photolysis of 50 μM Ru(bpy)$_3^{2+}$, 5 mM Na$_2$S$_2$O$_8$, and 100 μM **Co6** in 50 mM phosphate buffer at pH 8; b) kinetic traces at 450 nm at different concentrations of **Co6** (in the range 50–100 μM). It is worth mentioning that the local concentration of photogenerated Ru(bpy)$_3^{3+}$ is ca 10 μM, as estimated from the prompt ΔOD,[45] and thus guarantees the analysis under pseudo first order conditions with respect to **Co6**. The adopted conditions ([Ru(bpy)$_3^{3+}$] < [**Co6**]) favor thus the reactivity of a single Co-aquo group of **Co6**.

Figure 5. a) Observed rate constants (k_{obs}) obtained by laser flash photolysis of 50 μM Ru(bpy)$_3^{2+}$, 5 mM Na$_2$S$_2$O$_8$, and 0–100 μM **Co6** in 1–100 mM phosphate buffer at pH 8; b) dependence of the bimolecular ET rate (k) on phosphate buffer concentration.

(see equation 10 above). This value is comparable with those of other Co-POMs, for which bimolecular rate constants in the range 2.1–5.0·10^9 M^{-1}s^{-1} were estimated in phosphate buffer solutions at pH 8.[19]

It is worth noting that the bimolecular rate constant k measured at pH 8 decreases with increasing the concentration of phosphate buffer in the range 1–100 mM, reaching a plateau at the largest value tested (Figure 5; a comparable trend is observed also at pH 7, see Figure S13 in Supporting Information). According to the Debye-Eigen theory,[51,52] in the case of charged reactants the diffusion rate constant is expected to depend on the ionic strength of the solution, and in particular for reactants with opposite charges the rate constant k is expected to decrease upon increasing ionic strength.[53] Thus, in the case of **Co6**→Ru^{III}(bpy)$_3^{3+}$ ET, the trend observed in Figure 5b is fully consistent with theoretical predictions and strongly points towards a pivotal role of ionic interactions on the electron transfer kinetics in POM-based photochemical systems with Ru(bpy)$_3^{3+}$, in particular for the formation of the encounter complex.

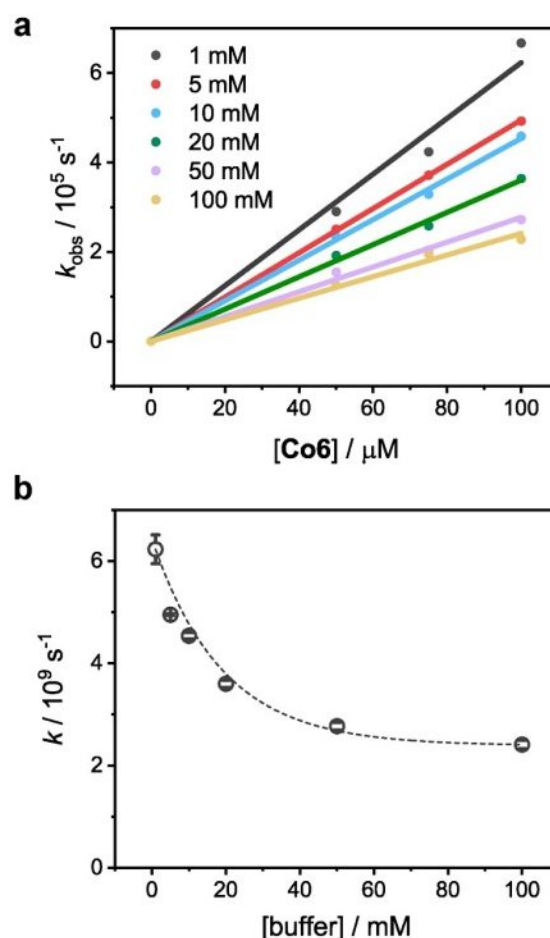## 2.4. PCET Mechanism Involving Co6(II)—OH$_2$

While the reactivity of **Co6(II)—OH** foresees a simple ET to Ru(bpy)$_3^{3+}$, a PCET event is expected when the one electron oxidation of the **Co6(II)—OH$_2$** species is involved (eq. 12, see also the Pourbaix diagram in Figure 3 and Scheme 1).

Since the Ru(bpy)$_3^{3+/2+}$ couple is not associated with proton exchange and cannot provide a suitable proton acceptor site, the role of a base B should be accounted, whereby B can be H$_2$O, OH$^-$ or the buffer base in the reaction medium. Therefore, the process can be described as a multiple-site PCET (or in alternative a bidirectional PCET),[54,55] in which electron and proton transfer occurs to different acceptors (eq. 12).[2]

$$Co6(II) - OH_2 + Ru(bpy)_3^{3+} + B \rightarrow$$
$$Co6(III) - OH + Ru(bpy)_3^{2+} + BH^+ \tag{12}$$
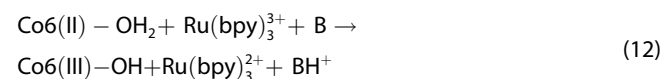
Hence, to get a deeper insight into the PCET process involving Ru^{III}(bpy)$_3^{3+}$ and **Co6(II)—OH$_2$**, laser flash photolysis studies have been performed under different experimental conditions by evaluating the effect of pH, type, and concen-

ChemPhysChem

Articles
doi.org/10.1002/cphc.202100190

Chemistry
Europe
European Chemical
Societies Publishing

tration of buffer. To disentangle the effect of the ionic strength on the diffusion constant (see above), the experiments have been conducted in the presence of 0.1 M Na_2SO_4 employing acetate buffer (5–100 mM) at pH 3.9 and 5.0 (Figure S14 and 6c, respectively), phosphate buffer (5–100 mM) at pH 6.2, 7.1 and 8 (Figure S15, S16, and S17 respectively), and borate buffer (5-100 mM) at pH 8.5 (Figure S18), using a fixed concentration of both $Ru(bpy)_3^{2+}$ and **Co6** (50 and 100 μM, respectively). Deuterated acetate buffers (50 mM) at pD 4.6 and 5.2 have been also employed to evaluate possible kinetic isotope effects (Figure S19).

From a close inspection of the kinetic traces, the main observations can be summarized as follows:

i) The rate constant of bleach recovery (k_{obs}) and the derived value of k, measured at a constant buffer concentration (50 mM, Figure 6a), depend markedly on the pH of the aqueous medium and decrease almost linearly when moving from alkaline to acidic values. Notably, at $pH < 7$ when **Co6(II)**–**OH$_2$** is prevalent in solution, the derived k values (Figure 6b) are significantly below the diffusional limit: accordingly, kinetic analysis can be profitably applied to extract meaningful mechanistic information on the PCET event between $Ru^{III}(bpy)_3^{3+}$ and **Co6(II)**–**OH$_2$** (vide infra).

ii) At $pH < 6$ the ΔOD recovery at 450 nm is not complete (Figure 6a). This observation indicates that the conversion of $Ru(bpy)_3^{3+}$ to $Ru(bpy)_3^{2+}$ is not quantitative, suggesting that the reaction between $Ru(bpy)_3^{3+}$ and **Co6(II)**–**OH$_2$** (prevalent under these conditions), eq. 12, should be better considered as an equilibrium rather than an irreversible process,[56] controlled by the redox potentials of the Ru-$(bpy)_3^{3+}/Ru(bpy)_3^{2+}$ and **Co6(III)**–**OH/Co6(II)**–**OH$_2$** couples (see above discussion and Figure 3).

iii) In every medium employed, the kinetics of the bleaching recovery are almost superimposable at all buffer concentrations tested (as a selected example, see Figure 6c for the kinetics in acetate buffer at pH 5.0; Figures S14–S18 in supporting information collect the traces in all the other media employed). Consistently, the k determined from the fitting and kinetic analysis turn out to be unaffected by the concentration of the buffer base (Figure 6d). This is a markedly different behavior with respect to that observed for ET to $Ru^{III}(bpy)_3^{3+}$ from Co_3O_4 nanoparticles, where a linear trend of the ET rate was observed depending on the concentration of the buffer base and ascribed to a buffer base-assisted proton-coupled electron transfer (PCET) from Co^{III}–OH sites.[22]
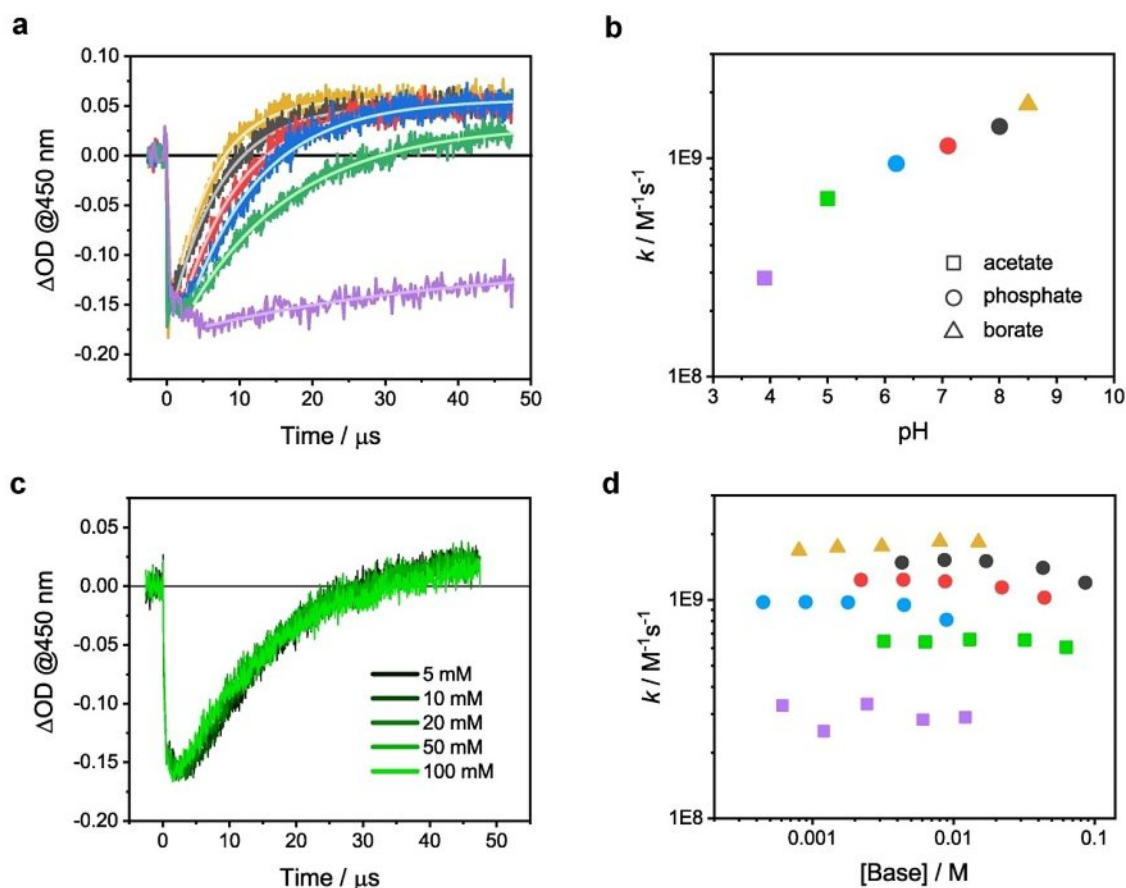
Figure 6. a) Kinetic traces at 450 nm obtained by laser flash photolysis of 50 μM $Ru(bpy)_3^{2+}$, 5 mM $Na_2S_2O_8$, 100 μM **Co6**, 0.1 M Na_2SO_4 and 50 mM buffer (see legend and color code in Figure 6b for buffer type and pH); b) k (in logarithmic scale) vs pH as obtained from the kinetic traces in Figure 6a; c) Kinetic traces at 450 nm obtained by laser flash photolysis of 50 μM $Ru(bpy)_3^{2+}$, 5 mM $Na_2S_2O_8$, 100 μM **Co6**, 0.1 M Na_2SO_4 and 5–100 mM acetate buffer at pH 5.0; d) k vs. buffer base concentration for all experimental conditions tested.

ChemPhysChem

Articles
doi.org/10.1002/cphc.202100190

**Chemistry
Europe**
European Chemical
Societies Publishing

iv) In deuterated medium (deuterated acetate buffer, pD 4.6 and 5.2), the bimolecular rate constants (k) are lower, with an estimated H/D kinetic isotope effect (KIE) of ~1.4 and ~1.2 at pD 4.6 and 5.2, respectively (Figure S19).[57]

v) A slight, but systematic decrease of the k is observed at large buffer concentration (>100 mM), particularly when phosphate is used as a buffer, suggesting a sort of inhibition effect exerted by the buffer anions (anation), likely involving coordination to the cobalt centers and concomitant deactivation of the redox site.[22]

The oxidation of **Co6(II)—OH₂** by $Ru^{III}(bpy)_3^{3+}$ (eq. 12) through a PCET is worth of further discussion, by addressing the mechanistic requirements. The PCET can indeed occur through three limiting mechanisms:[58–60] (i) stepwise electron transfer / proton transfer (ET-PT); (ii) stepwise proton transfer/ electron transfer (PT-ET); (iii) concerted proton-electron transfer (CPET).[2,4] In acetate buffer (pH 3.9–5.0), pathway (i) and (ii) are strongly unfavorable according to the predicted high potential of the **Co6(III)—OH₂/Co6(II)—OH₂** couple (unaffordable for $Ru^{III}(bpy)_3^{3+}$ oxidant) and to unfavorable deprotonation of **Co6 (II)—OH₂** at pH far below its pK_a, respectively.[57] Therefore, the most plausible route to by-pass high energy intermediates, foresees the involvement of the CPET pathway (iii), that is also consistent with the observed KIE (Figure S19).[57]

Although favorable from thermodynamic aspects with respect to the stepwise pathways (by avoiding the formation of high energy intermediates), CPET may suffer from kinetic penalties, associated to the displacement of the proton[1,16,58–60] by the base B, that should be located at a suitable distance from the **Co6(II)—OH₂** moiety, possibly through the formation of a hydrogen bond.[1,16,58–60] According to the libido rule, the pK_a of the BH⁺/B couple should be intermediate between the pK_a of **Co6(III)—OH₂/Co6(III)—OH** and of **Co6(II)—OH₂/Co6(II)—OH** couples.[43,61] The absence of effect of acetate concentration on the experimentally observed k_{obs} and on the derived k values seems to exclude base catalysis by acetate ($pK_a = 4.75$ for acetic acid/acetate). Since the involvement of OH⁻ in this pH range can be neglected considering its intrinsically small concentration, the most likely scenario foresees oxidation of **Co6(II)—OH₂** by photogenerated $Ru^{III}(bpy)_3^{3+}$ taking place via a CPET with water acting as the base[62] ($pK_a = 0$ for H_3O^+/H_2O; this should imply a $pK_a < 0$ for the **Co6(III)—OH₂/Co6(III)—OH** couple, that is reasonable according to the ΔpK_a of 9–10 units for aquo moieties bound to metals in the III and II oxidation states).[2,43] The hypothesis of water acting as the base in the CPET is further supported by the observation of the $Ru^{III}(bpy)_3^{3+}$ reduction by **Co6(II)—OH₂** occurring also in the absence of buffer, with a $k = 6.9 \cdot 10^8 \, M^{-1} s^{-1}$ (Figure S20). As a matter of fact, the occurrence of an intramolecular CPET involving the terminal oxo groups of the polyoxometalate scaffold can be ruled out given the lower basicity of these W=O sites.[63–65]

In this scenario, a structural pre-organization of water molecules in the proximity of the cobalt sites, assisted by the polyoxometalate scaffold of **Co6** plays a key role. The establishment of hydrogen bond networks including the Co-aquo moiety as donor offers a suitable supramolecular platform to promote the forward CPET process (Scheme 3, left).[3]
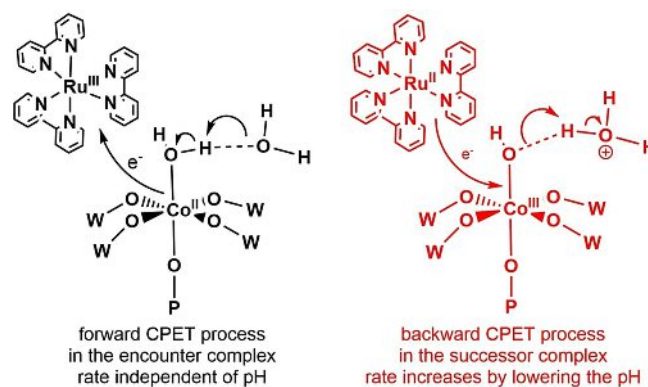
Scheme 3. Schematic representation of the CPET from **Co6(II)—OH₂** to $Ru(bpy)_3^{3+}$ with hydrogen bonded water acting as a base and assisting the removal of the proton from the Co-aquo moiety (forward process, left) and backward CPET from $Ru(bpy)_3^{2+}$ to **Co6(III)—OH** (backward process, right) where the k_{-2} constant is expected to show pH dependence.

2.5. pH Dependence of k

As a final remark, the dependence of the overall k on pH (Figure 6b) could be surprising at first sight, since CPET processes with water acting as a base, as the one represented in Scheme 3 (left), are expected to have a rate that is independent of pH.[1,58–60]

A plausible hypothesis for the experimental observation shown in Figure 6b can thus be the increasing competition of the reverse process, namely the backward CPET within the successor complex (Scheme 3, right).[66] The rate of the backward CPET is indeed expected to increase by decreasing the pH (since H_3O^+ is a reactant of the backward CPET) and thus supports the overall decrease of the determined k versus the pH shown in Figure 6b.[1,58–60]

Consistently, the experimental trend of k in the entire pH range explored (3.9–8.5) can be fitted considering the contribution of both **Co6(II)—OH₂** and **Co6(II)—OH** (associated to k' and k'', respectively), depending on their relative concentrations (associated to the acid dissociation constant of **Co6(II)—OH₂**, $K_a = 10^{-pKa} = 10^{-7.6}$), equations 13–15:

$$k = \frac{\{[Co6(II)-OH_2] \times k' + [Co6(II)-OH] \times k''\}}{[Co6]} \quad (13)$$

$$[Co6(II)-OH_2] = [Co6] \times \frac{[H_3O^+]}{(K_a + [H_3O^+])} \quad (14)$$

$$[Co6(II)-OH] = [Co6] \times \frac{K_a}{(K_a + [H_3O^+])} \quad (15)$$

and by considering the following assumptions:

(i) k'' (for **Co6(II)—OH**) being diffusion controlled, according to the experimental evidence previously discussed;

(ii) k' (for **Co6(II)—OH₂**) being expressed according to eq. 9 above;

ChemPhysChem

Articles
doi.org/10.1002/cphc.202100190

**Chemistry
Europe**
European Chemical
Societies Publishing

(iii) k_{-2}' being expressed as pH dependent from an exponential coefficient α, according to eq. 16:

$$k_{-2}' = A \times 10^{-\alpha \times pH} \tag{16}$$

the expression of the overall k thus results in eq. 17:

$$k = \frac{\left\{ \begin{array}{c} [Co6(II)-OH_2] \times \frac{k_1'}{[1+(1+A\times 10^{-\alpha\times pH}/k_3') \times k_{-1}'/k_2']} + \\ [Co6(II)-OH] \times k_1'' \end{array} \right\}}{[Co6]} \tag{17}$$

Equation 17 is found to fit the experimental data, providing an optimal description of the steady decrease of the k values at decreasing pH (Figure 7, solid red trace; the rate constant k is expressed in logarithmic scale; the details of the fitting are reported in Supporting Information). Indeed, the resulting curve can be described as the sum of the two separate contributions by **Co6—OH₂** (dashed blue trace, CPET mechanism, prevalent at pH < pKₐ) and by **Co6—OH** (dashed green trace, ET mechanism, prevalent at pH > pKₐ).

The fitting identifies a value of the exponential coefficient $\alpha = 0.69$, regulating the dependence of log(k) vs pH, within the linear regime observed at pH < 4.5 (dashed red line in Figure 7).

A linear dependence of log(k) vs pH with slope in the range 0.15–0.50 has been previously observed for light induced, water assisted CPET in covalently linked Ru(bpy)$_3{}^{2+}$/tyrosine or tryptophan systems.[62,67] Although the origin of such weak pH dependence ($\alpha < 1$) of log(k) is not clearly understood,[6] this behavior supports the CPET mechanism envisioned herein (Scheme 3).[6]
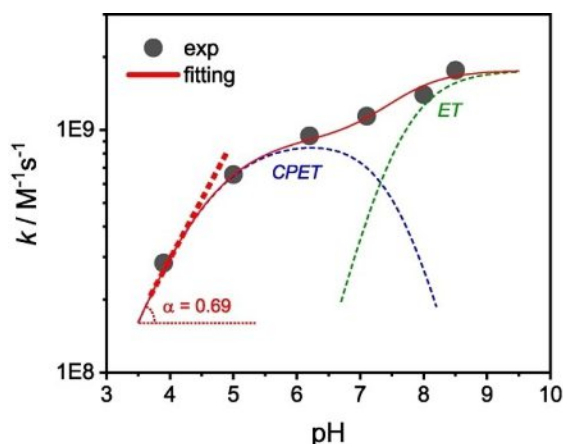
3. Conclusions

In this work, laser flash photolysis studies have been used to address the dynamics of ET involving the cobalt-substituted polyoxotungstate **Co6** triggered by photogenerated Ru^{III}-(bpy)$_3{}^{3+}$. The results show that: (i) the ET process yields a Co(III)—OH moiety (**Co6(III)—OH**), either starting from a Co(II) aquo or Co(II) hydroxo forms of **Co6** (abbreviated as **Co6 (II)—OH₂** and **Co6(II)—OH**, respectively, and associated to a pKₐ of 7.6); (ii) the **Co6(II)—OH→Ru^{III}(bpy)$_3{}^{3+}$** ET occurs in alkaline aqueous solution (pH 8) via bimolecular kinetics, with rate constants k close to the diffusion limit (in the range 2–6·10^9 M^{-1}s^{-1}) and dependent on the ionic strength of the medium, as expected for bimolecular reactions between charged species; (iii) when **Co6(II)—OH₂** is involved (pH < 7), the k fall significantly below the diffusional limit, thus implying that the elementary step within the encounter complex is rate determining. This involves a multiple site concerted proton-electron transfer (**Co6(II)—OH₂→Co6(III)—OH**) where water acts as a base, as shown by the absence of effect of buffer base concentration on the k_{obs}, by a KIE in the range of 1.2–1.4, and by the peculiar dependence of k on pH. The organization of water channels at the POM surface and engaging hydrogen bonds with the **Co6(II)—OH₂** group, is a key structural feature to assist the proton transfer event. The comprehension of the mechanistic details of the electron transfer processes involving this class of compounds is thus pivotal in the design of photosynthetic schemes for small molecule activation, requiring a tailored functionalization of the second sphere interactions for promoting low energy CPET mechanisms.

Experimental Section

See the Supporting Information for full experimental details on synthetic and characterization procedures, and of the models of the kinetic treatments in equations 9 and 17.

List of abbreviations

Bpy = 2,2'-bipyridine; ET = electron transfer; PT = proton transfer; PCET = proton coupled electron transfer; CPET = concerted proton electron transfer; KIE = kinetic isotope effect; **Co6** = [Co$_6$(H$_2$O)$_2$(α-B-PW$_9$O$_{34}$)$_2$(PW$_6$O$_{26}$)]$^{17-}$; **Co6(II)—OH₂** = Co(II)-aquo site in **Co6**; **Co6 (II)—OH** = Co(II)-hydroxo site in **Co6**; **Co6(III)—OH** = Co(III)-hydroxo site in **Co6**; POM = polyoxometalate; NHE = normal hydrogen electrode.

Figure 7. Dependence of k (in logarithmic scale; black dots are the experimental data shown in Figure 6b) vs pH and related fitting (solid, red trace) considering both contributions from **Co6(II)—OH₂** (dashed blue line, CPET mechanism) and **Co6(II)—OH** (dashed green line, ET mechanism), whose speciation is related to a pKₐ = 7.6 (see the overall kinetic treatment in the Supporting Information). The dashed red line with a slope $\alpha = 0.69$ represents the dependence of log(k) vs pH at pH < 4.5, according to eq. 17.

Conflict of Interest

The authors declare no conflict of interest.

[1] J. M. Savéant, *Annu. Rev. Anal. Chem.* **2014**, *7*, 537–560.

[2] a) D. R. Weinberg, C. J. Gagliardi, J. F. Hull, C. F. Murphy, C. A. Kent, B. C. Westlake, A. Paul, D. H. Ess, D. G. McCafferty, T. J. Meyer, *Chem. Rev.* **2012**, *112*, 4016–4093; b) J. L. Dempsey, J. R. Winkler, H. B. Gray, *Chem. Rev.* **2010**, *110*, 7024–7039; c) A. Pannwitz, O. S. Wenger, *Dalton Trans.* **2019**, *48*, 5861–5868; d) A. Pannwitz, O. S. Wenger, *Chem. Commun.* **2019**, *55*, 4004–4014; e) M. Natali, A. Amati, S. Merchiori, B. Ventura, E. Iengo, *J. Phys. Chem. C* **2020**, *124*, 8514–8525; f) M. Natali, A. Amati, N. Demitri, E. Iengo, *Chem. Eur. J.* **2021**, DOI: 10/1002/chem202005487.

[3] a) C. J. Chang, M. C. Y. Chang, N. H. Damrauer, D. G. Nocera, *Biochim. Biophys. Acta Bioenerg.* **2004**, *1655*, 13–28; b) P. Goyal, S. Hammes-Schiffer, *ACS Energy Lett.* **2017**, *2*, 512–519.

[4] a) G. A. Parada, Z. K. Goldsmith, S. Kolmar, B. P. Rimgard, B. Q. Mercado, L. Hammarström, S. Hammes-Schiffer, J. M. Mayer, *Science* **2019**, *475*, 471–475; b) M. J. Chalkle, P. Garrido-Barros, J. C. Peter, *Science* **2020**, *369*, 850–854.

[5] J. J. Warren, J. M. Mayer, *Biochemistry* **2015**, *54*, 1863–1878.

[6] R. Tyburski, T. Liu, S. D. Glover, L. Hammarström, *J. Am. Chem. Soc.* **2021**, *143*, 560–576.

[7] M. Bonchio, Z. Syrgiannis, M. Burian, N. Marino, E. Pizzolato, K. Dirian, F. Rigodanza, G. A. Volpato, G. La Ganga, N. Demitri, et al., *Nat. Chem.* **2019**, *11*, 146–153.

[8] M. Natali, F. Nastasi, F. Puntoriero, A. Sartorel, *Eur. J. Inorg. Chem.* **2019**, 2027–2039.

[9] A. Volpe, C. Tubaro, M. Natali, A. Sartorel, G. W. Brudvig, M. Bonchio, *Inorg. Chem.* **2019**, *58*, 16537–16545.

[10] B. A. Moyer, T. J. Meyer, *Inorg. Chem.* **1981**, *20*, 436–444.

[11] C. Costentin, M. Robert, J.-M. Savéant, A.-L. Teillout, *Proc. Nat. Acad. Sci.* **2009**, *106*, 11829–11836.

[12] J. W. Darcy, B. Koronkiewicz, G. A. Parada, J. M. Mayer, *Acc. Chem. Res.* **2018**, *51*, 2391–2399.

[13] D. G. Nocera, *Acc. Chem. Res.* **2012**, *45*, 767–776.

[14] D. Wang, J. T. Groves, *Proc. Nat. Acad. Sci.* **2013**, *110*, 15579–15584.

[15] A. Juris, V. Balzani, F. Barigelletti, S. Campagna, P. Belser, A. von Zelewsky, *Coord. Chem. Rev.* **1988**, *84*, 85–277.

[16] a) J. Bonin, M. Routier, *Artif. Photosynth.* **2013**, *1*, 6–15; b) The quantum yield of 2 arises from the generation of two equivalents of Ru^{III}(bpy)$_3^{3+}$ for each absorbed photon, as a consequence of the dark process involving oxidation of Ru^{II}(bpy)$_3^{2+}$ by the sulfate radical SO$_4^{-}$, eq 3; persulfate is often preferred over other acceptors such as methyl viologen, due to the irreversibility of the electron transfer associated to breaking of the O−O bond.

[17] F. Bolletta, A. Juris, M. Maestri, D. Sandrini, *Inorg. Chim. Acta* **1980**, *44*, L175.

[18] A. Sartorel, M. Bonchio, S. Campagna, F. Scandola, *Chem. Soc. Rev.* **2013**, *42*, 2262–2280.

[19] M. Natali, I. Bazzan, S. Goberna-Ferrón, R. Al-Oweini, M. Ibrahim, B. S. Bassil, H. Dau, F. Scandola, J. R. Galán-Mascarós, U. Kortz, et al. *Green Chem.* **2017**, *19*, 2416–2426.

[20] I. Bazzan, A. Volpe, A. Dolbecq, M. Natali, A. Sartorel, P. Mialane, M. Bonchio, *Catal. Today* **2017**, *290*, 39–50.

[21] E. Pizzolato, M. Natali, B. Posocco, A. Montellano López, I. Bazzan, M. Di Valentin, P. Galloni, V. Conte, M. Bonchio, F. Scandola, et al., *Chem. Commun.* **2013**, *49*, 9941.

[22] G. A. Volpato, A. Bonetto, A. Marcomini, P. Mialane, M. Bonchio, M. Natali, A. Sartorel, *Sustain. Energy Fuels* **2018**, *2*, 1951–1956.

[23] H. Lv, Y. V. Geletii, C. Zhao, J. W. Vickers, G. Zhu, Z. Luo, J. Song, T. Lian, D. G. Musaev, C. L. Hill, *Chem. Soc. Rev.* **2012**, *41*, 7572.

[24] F. Jiao, H. Frei, *Angew. Chem. Int. Ed.* **2009**, *48*, 1841–1844.

[25] J. De Tovar, N. Romero, S. A. Denisov, R. Bofill, C. Gimbert-Suriñach, D. Ciuculescu-Pradins, S. Drouet, A. Llobet, P. Lecante, V. Colliere, et al., *MaterialsToday Energy* **2018**, *9*, 506–515.

[26] N. Shi, W. Cheng, H. Zhou, T. Fan, M. Niederberger, *Chem. Commun.* **2015**, *51*, 1338–1340.

[27] M. Grzelczak, J. Zhang, J. Pfrommer, J. Hartmann, M. Driess, M. Antonietti, X. Wang, *ACS Catal.* **2013**, *3*, 383–388.

[28] M. D. Ritorto, T. M. Anderson, W. A. Neiwert, C. L. Hill, *Inorg. Chem.* **2004**, *43*, 44–49.

[29] a) L. Yang, J. Zhao, J. Zhao, J. Niu, *J. Coord. Chem.* **2012**, *65*, 3363–3371; b) **Co6** is readily obtained as a first crystallization product of [Co$_4$(H$_2$O)$_2$(α-B-PW$_9$O$_{34}$)$_2$]$^{10-}$ (**Co4**), the first Co-POM combined with Ru^{III}(bpy)$_3^{3+}$ in water oxidation catalysis, and for which the investigation of Co→Ru^{III}(bpy)$_3^{3+}$ ET dynamics was complicated by the instability of **Co4** in solution, observing ET rates that changed over time (see ref. 33).

[30] W. Wu, T. Teng, X. Y. Wu, X. Dui, L. Zhang, J. Xiong, L. Wu, C. Z. Lu, *Catal. Commun.* **2015**, *64*, 44–47.

[31] S. J. Folkman, J. Soriano-Lopez, J. R. Galán-Mascarós, R. G. Finke, *J. Am. Chem. Soc.* **2018**, *140*, 12040–12055.

[32] Q. Yin, J. M. Tan, C. Besson, Y. V. Geletii, D. G. Musaev, A. E. Kuznetsov, Z. Luo, K. I. Hardcastle, C. L. Hill, *Science* **2010**, *328*, 342–345.

[33] M. Natali, S. Berardi, A. Sartorel, M. Bonchio, S. Campagna, F. Scandola, *Chem. Commun.* **2012**, *48*, 8808–8810.

[34] X. López, C. Nieto-Draghi, C. Bo, J. B. Avalos, J. M. Poblet, *J. Phys. Chem. A* **2005**, *109*, 1216–22.

[35] a) F. Leroy, P. Miró, J. M. Poblet, C. Bo, J. B. Ávalos, *J. Phys. Chem. B* **2008**, *112*, 8591–8599; b) A. Sartorel, M. Carraro, A. Bagno, G. Scorrano, M. Bonchio, *Angew. Chem. Int. Ed.* **2007**, *45*, 3255–3258.

[36] J. J. Stracke, R. G. Finke, *ACS Catal.* **2014**, *4*, 909–933.

[37] A. M. Ullman, Y. Liu, M. Huynh, D. K. Bediako, H. Wang, B. L. Anderson, D. C. Powers, J. J. Breen, H. D. Abruña, D. G. Nocera, *J. Am. Chem. Soc.* **2014**, *136*, 17681–17688.

[38] L. Lisnard, P. Mialane, A. Dolbecq, J. Marrot, J. M. Clemente-Juan, E. Coronado, B. Keita, P. De Oliveira, L. Nadjo, F. Sécheresse, *Chem. A Eur. J.* **2007**, *13*, 3525–3536.

[39] J. B. Gerken, J. G. McAlpin, J. Y. C. Chen, M. L. Rigsby, W. H. Casey, R. D. Britt, S. S. Stahl, *J. Am. Chem. Soc.* **2011**, *133*, 14431–14442.

[40] J. Chivot, L. Mendoza, C. Mansour, T. Pauporté, M. Cassir, *Corros. Sci.* **2008**, *50*, 62–69.

[41] A. Lewandowska-Andralojc, T. Baine, X. Zhao, J. T. Muckerman, E. Fujita, D. E. Polyansky, *Inorg. Chem.* **2015**, *54*, 4310–4321.

[42] C. A. Ohlin, S. J. Harley, J. G. McAlpin, R. K. Hocking, B. Q. Mercado, R. L. Johnson, E. M. Villa, M. K. Fidler, M. M. Olmstead, L. Spiccia, et al., *Chem. Eur. J.* **2011**, *17*, 4408–4417.

[43] A. Yamaguchi, R. Inuzuka, T. Takashima, T. Hayashi, K. Hashimoto, R. Nakamura, *Nat. Commun.* **2014**, *5*, 1–6.

[44] M. Burian, Z. Syrgiannis, G. La Ganga, F. Puntoriero, M. Natali, F. Scandola, S. Campagna, M. Prato, M. Bonchio, H. Amenitsch, et al., *Inorg. Chim. Acta* **2017**, *454*, 171–175.

[45] M. Natali, M. Orlandi, S. Berardi, S. Campagna, M. Bonchio, A. Sartorel, F. Scandola, *Inorg. Chem.* **2012**, *51*, 7324–7331.

[46] M. Natali, E. Deponti, D. Vilona, A. Sartorel, M. Bonchio, F. Scandola, *Eur. J. Inorg. Chem.* **2015**, *2015*, 3467–3477.

[47] M. Natali, F. Puntoriero, C. Chiorboli, G. La Ganga, A. Sartorel, M. Bonchio, S. Campagna, F. Scandola, *J. Phys. Chem. C* **2015**, *119*, 2371–2379.

[48] T. E. Keyes, E. Gicquel, L. Guerin, R. J. Forster, V. Hultgren, A. M. Bond, A. G. Wedd, *Inorg. Chem.* **2003**, *42*, 7897–7905.

[49] J. J. Walsh, D. L. Long, L. Cronin, A. M. Bond, R. J. Forster, T. E. Keyes, *Dalton Trans.* **2011**, *40*, 2038–2045.

[50] R. A. Marcus, *J. Phys. Chem.* **1968**, *72*, 891–899.

[51] P. Debye, *J. Electrochem. Soc.* **1942**, *82*, 265–277.

[52] M. Eigen, *Z. Physik. Chem.* **1954**, *1*, 176.

[53] C. Chiorboli, M. T. Indelli, M. A. R. Scandola, F. Scandola, *J. Phys. Chem.* **1988**, *92*, 156–163.

[54] M. Bourrez, R. Steinmetz, S. Ott, F. Gloaguen, L. Hammarström, *Nat. Chem.* **2015**, *7*, 140–145.

[55] M. D. Symes, Y. Surendranath, D. A. Lutterman, D. G. Nocera, *J. Am. Chem. Soc.* **2011**, *133*, 5174–5177.

[56] G. La Ganga, F. Puntoriero, S. Campagna, I. Bazzan, S. Berardi, M. Bonchio, A. Sartorel, M. Natali, F. Scandola, *Faraday Discuss.* **2012**, *155*, 177–190.

[57] J. Soetbeer, P. Dongare, L. Hammarström, *Chem. Sci.* **2016**, *7*, 4607–4612.

[58] C. Costentin, M. Robert, J. M. Savéant, *J. Am. Chem. Soc.* **2007**, *129*, 5870–5879.

[59] J. Bonin, C. Costentin, M. Robert, M. Routier, J. M. Savéant, *J. Am. Chem. Soc.* **2013**, *135*, 14359–14366.

[60] J. Bonin, C. Costentin, M. Robert, J. M. Savéant, C. Tard, *Acc. Chem. Res.* **2012**, *45*, 372–381.

[61] J. Medina-Ramos, O. Oyesanya, J. C. Alvarez, *J. Phys. Chem. C* **2013**, *117*, 902–912.

[62] P. Dongare, S. Maji, L. Hammarström, *J. Am. Chem. Soc.* **2016**, *138*, 2194–2199.

[63] I. V. Kozhevnikov, *Chem. Rev.* **1998**, *98*, 171–198.

[64] R. S. Drago, J. A. Dias, T. O. Maier, *J. Am. Chem. Soc.* **1997**, *119*, 7702–7710.

[65] S. S. Wang, G. Y. Yang, *Chem. Rev.* **2015**, *115*, 4893–4962.

[66] The rising contribution of the backward process at low pH is fully consistent with the establishment of the equilibrium between the Ru(bpy)$_3$$^{3+}$/Ru(bpy)$_3$$^{2+}$ and **Co6(III)─OH/Co6(II)─OH$_2$** couples, as previously discussed.

[67] T. Irebo, M.-T. Zhang, T. F. Markle, A. M. Scott, L. Hammarström, *J. Am. Chem. Soc.* **2012**, *134*, 16247–16254.